Surrogate model for condition assessment of structures using a dense sensor network

Jin Yan, Xiaosong Du, Austin Downey, Alessandro Cancelli, Simon Laflamme, et al.

Surrogate model for condition assessment of structures using a dense sensor network

Jin Yan[a,*], Xiaosong Du[b], Austin Downey[a,c], Alessandro Cancelli[a], Simon Laflamme[a,d], Leifur Leifsson[b], An Chen[a], and Filippo Ubertini[e]

[a]Department of Civil, Construction and Environmental Engineering, Iowa State University, Ames, IA, USA
[b]Department of Aerospace Engineering, Iowa State University, Ames, IA, 50010, USA
[c]Department of Mechanical Engineering, Iowa State University, Ames, IA, 50010, USA
[d]Department of Electrical and Computer Engineering, Iowa State University, Ames, IA, 50010, USA
[e]Department of Civil and Environmental Engineering, University of Perugia, Perugia, 14071, Italy

ABSTRACT

Condition assessment of civil infrastructures is difficult due to technical and economic constraints associated with the scaling of sensing solutions. When scaled appropriately, a large sensor network will collect a vast amount of rich data that is difficult to directly link to the existing condition of the structure along with its remaining useful life. This paper presents a methodology to construct a surrogate model enabling diagnostic of structural components equipped with a dense sensor network collecting strain data. The surrogate model, developed as a matrix of discrete stiffness elements, is used to fuse spatial strain data into useful model parameters. Here, strain data is collected from a sensor network that consists of a novel sensing skin fabricated from large area electronics. The surrogate model is constructed by updating the stiffness matrix to minimize the difference between the model's response and measured data, yielding a 2D map of stiffness reduction parameters. The proposed method is numerically validated on a plate equipped with 40 large area strain sensors. Results demonstrate the suitability of the proposed surrogate model for the condition assessment of structures using a dense sensor network.

Keywords: dense sensor network, strain, model updating, condition assessment, structural health monitoring, surrogate model

1. INTRODUCTION

The deteriorating condition of civil infrastructures is a source of significant concern for their owners and operators. The evaluation of structural condition is typically conducted via visual inspection,[1] and sometime non-destructive evaluation (NDE) techniques are leveraged to enhance the ability of inspectors to detect damage.[2] However, visual inspections are left to the inspector's judgement, may pose safety hazards, and are expensive and labor-intensive.[3,4] A solution is to automate the process of condition assessment, known as structural health monitoring (SHM).

A notable challenge in SHM is to link sensor data to structural conditions. Research counts several examples of vibration-based SHM using limited sensors for condition assessment.[5–8] Vibration-based SHM is typically conducted by identifying a change in the structure's global characteristics provoked by a local damage, which may be difficult to apply in the field due to the numerous frequency components present in a complex structure.[9] Since strain is a direct indicator of, and sensitive to, damage, the monitoring of a structure's strain fields using strain sensors has attracted considerable attention in recent years.[10] In an effort to monitor the global area of a large-scale structure, distributed sensing technologies have been investigated for the distinction of local from

---

Further author information: (Send correspondence to Jin Yan)
Jin Yan: E-mail: yanjin@iastate.edu

global damage. One example of distributed sensing technologies that have gained broad acceptance is the use of fiber optic sensors due to their unique capability of monitoring one-dimensional strain fields at a large number of discrete points. However, fiber optic sensors are not highly deployed for monitoring infrastructure due to the fragility of the fibers and high deployment cost.[11,12]

In order to improve the spatial resolution of distributed sensing technologies, it is becoming feasible to deploy a two dimensional array of densely spaced sensors. Strain sensing sheets based on large area electronics were developed for fatigue crack detection and localization.[13] Carbon nanotube sensors have been demonstrated for the detection of large strains and cracks.[14] Along with this effort, the authors have developed a scalable and cost-effective flexible skin-like membrane for the monitoring of structural components.[15,16] This technology is analogous to sensing skin because it mimics biological skin's capability to detect local damage over a global area. It is based on a large area strain-sensitive sensor termed soft elastomeric capacitor (SEC).[15] In contrast with fiber optic sensors, vibrating wire, or traditional resistive strain gauges that measure strain at discrete points, the soft elastomeric capacitor (SEC) has the unique capability of measuring the additive in-plane strain over a large and customizable area. Previous research related to the SEC has decomposed the SEC's additive strain into two uni-directional strain components and used these strain components to reconstruct uni-directional strain maps over the monitored surface[17] for damage detection through a visual interpretation of changes in strain fields.[16]

The objective of this paper is to introduce an algorithm to link strain map data to structural conditions. At this preliminary stage, we develop a physics-driven approach to reconstruct the stiffness matrix of a component equipped with sensing skin. Others have already proposed physics-driven approaches with model updating based on sensor data. Sanayei et al. proposed an iterative technique using static strain data to identify beam- and frame-like structural element properties.[18,19] Others have reconstructed displacement and stress field from discrete strain measurements employing an inverse finite element method to assess structural integrity.[20] A substructure model updating approach using frequency domain data was proposed to identified structural stiffness and mass elements.[21] Also, a stochastic subspace identification technique was used to extract modal information from acceleration data and a genetic algorithm was used to reconstruct the stiffness matrix that would match these parameters.[22]

The novelty of this paper resides in the development of the physics-based algorithm that could be later transformed into a hybrid model/data approach enabling fast reconstruction of physical representation, in real-time. Such reconstructions could be readily used for damage detection, localization, quantification, and condition evaluation. In particular, we exploit a physically representative surrogate model based on a Mindlin finite elements to harness additive strain measurements of the SEC. Upon the static forces applied to the plate, the stiffness can be reconstructed from the surface additive strain measurements by minimizing the difference between the estimated and observed responses.

The paper is organized as follows. First, the sensing principle of the SEC is reviewed. Second, the formulation of the physics-driven surrogate model is explained. Third, the algorithm is demonstrated through a numerical simulation. Last, the paper is concluded.

2. BACKGROUND

The previously proposed sensing skin is constituted from a network of strain sensors. These sensors, or SECs, are large area capacitors suitable for strain sensing over large-scale surfaces. The sensor's fabrication procedure, sensing characteristics, and its electromechanical models have been studied in detail in previous works.[23,24] Briefly, the SEC is built using a layer-by-layer approach where a dielectric (white layer of the capacitor shown in Figure 1(a)) is fabricated from a styrene-ethylene-butadiene-styrene (SEBS) polymer matrix filled with titania. The conductive layers are painted from a conductive paint fabricated using the same SEBS matrix but filled with carbon black. The capacitance (C) of an SEC can be estimated from the equation for a parallel plate capacitor (assuming negligible losses):

$$C = \varepsilon_0 \varepsilon_r \frac{A}{h} \tag{1}$$
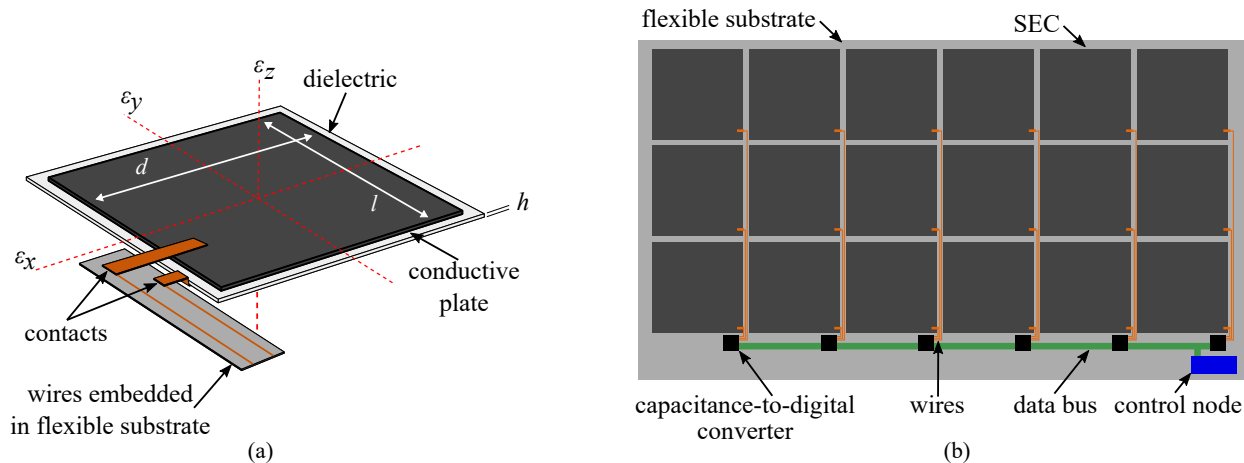
Figure 1. The proposed SEC-based sensing skin showing the: (a) SEC with key components annotated; and (b) example of sensing skin layout with key components annotated.

where ε_0 is the vacuum permittivity ($\varepsilon_0 = 8.854$pF/m), ε_r is the relative permittivity of the dielectric, A is the electrode's surface area of width w and length l, and h is the thickness of the dielectric. Assuming that the capacitor undergoes small strain, the change in capacitance is related to the additive in-plane strains $\varepsilon_x + \varepsilon_y$ with a gauge factor $\lambda \approx 2$:[24]

$$\frac{\triangle C}{C_0} = \lambda(\varepsilon_x + \varepsilon_y) \tag{2}$$

An example layout for the sensing skin is shown in Figure 1(b). This fully integrated skin consists of SECs deployed on a flexible polyimide sheet along with the necessary electronics. A more detailed discussion regarding on the electronics can be found in reference.[16]

3. SURROGATE MODEL FORMULATION

A surrogate model is constructed by simplifying the structural behavior of the component of interest, here a plate. The plate is discretized into four-node quadrilateral Mindlin elements,[25] with an SEC in the center of each element. A graphical representation of the element is shown in Figure 2. Assuming a static load, the governing equation for the surrogate model, expressed as $\mathbf{F} = \mathbf{KU}$, is based on the static stiffness relationship between the force vector $\mathbf{F}$, the stiffness matrix $\mathbf{K}$, and displacement vector $\mathbf{U}$. Vector $\mathbf{U}$ is related to the measured additive strain through a transformation matrix $\mathbf{B}$. Once the surrogate model is constructed, an optimization function can be defined such that it minimizes the error between the strain predicted by the surrogate model and the strain measured by the SECs through the alteration of the $\mathbf{K}$ matrix. Matrix $\mathbf{K}$ is recursively refined until the error converges . The processes is outlined in Figure 3. The production of a surrogate model enables greater computational efficiency, which can be useful in conducting condition assessment, structural predictions, and remaining useful life estimations.
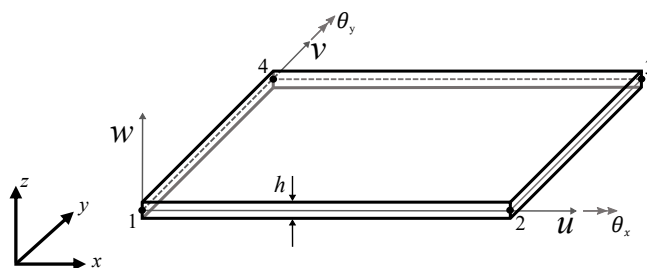
Figure 2. Illustration of the Mindlin element with four nodes located on the mid-line of the element.
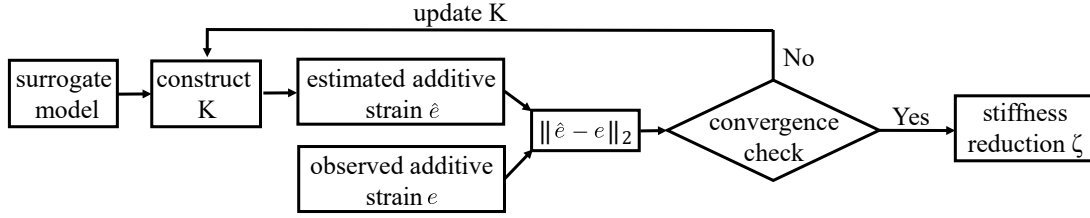
Figure 3. Flowchart of the proposed physics-driven algorithm.

3.1 Model formulation

At this preliminary stage of the research, the model formulation assumes a static load of known location and magnitude, and is based on work from.[18,20] The discretized displacement vector $\mathbf{u}^e$ and stiffness matrix $\mathbf{k}^e$ is constructed for each element, where $e = 1, 2, \ldots,$ NEM with NEM being the total number of elements in the surrogate model. Using the Cartesian coordinate system, $\mathbf{u}^e$ fully defines the deformation of a four-node quadrilateral element as shown in Figure 2. Each element comprises three independent degrees-of-freedom (DOFs) θ_x, θ_y, and w, resulting in 12 DOFs for the four nodes:

$$\mathbf{u}^e = \begin{bmatrix} \theta_{x1} & \theta_{y1} & w_1 & \theta_{x2} & \theta_{y2} & w_2 & \theta_{x3} & \theta_{y3} & w_3 & \theta_{x4} & \theta_{y4} & w_4 \end{bmatrix}^{\mathrm{T}} \tag{3}$$

where w is the mid-surface deflection in the z axis, $\theta_x = z\partial w/\partial x$ and $\theta_y = z\partial w/\partial y$ are the transverse bending rotations with respect to the x and y axes, respectively. Vector $\mathbf{u}^e$ can be approximated from geometry using the bilinear quadrilateral shape functions $N_i(i = 1, 2, 3, 4)$

$$\theta_x = \sum_{i=1}^{4} N_i\theta_{xi}; \quad \theta_y = \sum_{i=1}^{4} N_i\theta_{yi}; \quad w = \sum_{i=1}^{4} N_i w_i \tag{4}$$

The surface bending strains $\varepsilon_{\mathrm{x}}, \varepsilon_{\mathrm{y}}$ and in-plane shear strain γ_{xy} for each element can be obtained based on three-dimensional elasticity:

$$\mathbf{e}_{\mathrm{b}}^e = \begin{bmatrix} \varepsilon_{\mathrm{x}} \\ \varepsilon_{\mathrm{y}} \\ \gamma_{\mathrm{xy}} \end{bmatrix} = \frac{h}{2} \begin{bmatrix} \frac{\partial \theta_{\mathrm{x}}}{\partial x} \\ \frac{\partial \theta_{\mathrm{y}}}{\partial y} \\ \frac{\partial \theta_{\mathrm{y}}}{\partial x} + \frac{\partial \theta_{\mathrm{x}}}{\partial y} \end{bmatrix} = \frac{h}{2} \mathbf{B}_{\mathrm{b}} \mathbf{u}^e \tag{5}$$

where $\mathbf{B}_{\mathrm{b}}$ is a transformation matrix. To relate to SEC data, the bending strains in the plate are converted from the displacement vector ($\mathbf{u}^e$) by differentiating the shape functions through the transform matrices $\mathbf{B}_{\mathrm{b}}$:

$$\mathbf{B}_{\mathrm{b}} = \begin{bmatrix} 0 & \frac{N_1}{\partial x} & 0 & \ldots & 0 & \frac{N_4}{\partial x} & 0 \\ 0 & 0 & \frac{N_1}{\partial y} & \ldots & 0 & 0 & \frac{N_4}{\partial y} \\ 0 & \frac{N_1}{\partial y} & \frac{N_1}{\partial x} & \ldots & 0 & \frac{N_4}{\partial y} & \frac{N_4}{\partial x} \end{bmatrix} \tag{6}$$

Also, the out-of-plane shear strains $\mathbf{e}_{\mathrm{s}}$ can be written:

$$\mathbf{e}_{\mathrm{s}}^e = \begin{bmatrix} \gamma_{xz} \\ \gamma_{yz} \end{bmatrix} = \begin{bmatrix} \frac{\partial w}{\partial x} + \theta_x \\ \frac{\partial w}{\partial y} + \theta_y \end{bmatrix} = \mathbf{B}_{\mathrm{s}} \mathbf{u}^e \tag{7}$$

along with the strain-displacement shear transformation matrix $\mathbf{B}_{\mathrm{s}}$:

$$\mathbf{B}_{\mathrm{s}} = \begin{bmatrix} \frac{N_1}{\partial x} & N_1 & 0 & \ldots & \frac{N_4}{\partial x} & N_4 & 0 \\ \frac{N_1}{\partial y} & 0 & N_1 & \ldots & \frac{N_4}{\partial x} & 0 & N_4 \end{bmatrix} \tag{8}$$

where $\mathbf{B}_\mathrm{s}$ can be obtained for each element from the three-dimensional elasticity. It is noted that only the additive surface axial strains can be experimentally measured by the SEC (i.e. the shear strains cannot be directly obtained from the SEC). However, for a thin plate, the shear strains can be neglected due to their relatively small magnitudes when compared to the bending strains.[26]

After the element stiffness matrix that governs the structural behavior of the plate is constructed as a function of Youngs modulus (E), Poissons ratio (ν), and shear modulus ($G = \frac{E}{2(1+\nu)}$). The element stiffness matrix, $\mathbf{k}^e$, is built using the principle of minimum potential energy using the Gauss quadrature technique with a two point integration for bending and one point integration for shear to avoid shear locking.[25] Once the elemental stiffness matrix is constructed, the stiffness matrix for one element can be expressed:

$$\mathbf{k}^e = \frac{h^3}{12} \int_{A^e} \mathbf{B}_b^\mathrm{T} \mathbf{D}_\mathrm{b} \mathbf{B}_\mathrm{b} dA^e + \alpha h \int_{A^e} \mathbf{B}_\mathrm{s}^\mathrm{T} \mathbf{D}_\mathrm{s} \mathbf{B}_\mathrm{s} dA^e, \tag{9}$$

where α is the shear correction factor taken as $5/6$,[25] $\mathbf{D}_\mathrm{b}$ is the constitutive equation for bending:

$$\mathbf{D}_\mathrm{b} = \frac{E}{1-\nu^2} \begin{bmatrix} 1 & \nu & 0 \\ \nu & 1 & 0 \\ 0 & 0 & \frac{1-\nu}{2} \end{bmatrix} \tag{10}$$

and $\mathbf{D}_\mathrm{s}$ is the shear constitutive equation matrix:

$$\mathbf{D}_\mathrm{s} = \begin{bmatrix} G & 0 \\ 0 & G \end{bmatrix} \tag{11}$$

By introducing the displacement vector $\mathbf{u}^e$ and stiffness matrix $\mathbf{k}^e$ into the element-wise governing equation of the surrogate model $\mathbf{f}^e = \mathbf{k}^e \mathbf{u}^e$, the bending strains of one element ($\mathbf{e}_\mathrm{b}^e$) can be obtained assuming $\mathbf{f}^e$ is known:

$$\mathbf{e}_\mathrm{b}^e = \mathbf{B}_\mathrm{b}[\mathbf{k}^e]^{-1}\mathbf{f}^e \tag{12}$$

For a linear system, only the additive strains are measured by the SEC. It follows that the system's overall bending strain vector ($\mathbf{e}_\mathrm{b}$) and transformation matrix ($\mathbf{B}_\mathrm{b}$) for the measured and unmeasured strains can be rearranged as:

$$\left[\frac{\mathbf{e}_\mathrm{measured}}{\mathbf{e}_\mathrm{unmeasured}} \right] = \left[\frac{\mathbf{B}_\mathrm{measured,b}}{\mathbf{B}_\mathrm{unmeasured,b}} \right] \mathbf{K}^{-1}\mathbf{F} \tag{13}$$

Because the unmeasured strains are not required for estimating the measured strain, they can be removed from Equation 13, with

$$\hat{\mathbf{e}} = \mathbf{B}_\mathrm{measured,b}\mathbf{K}^{-1}\mathbf{F} \tag{14}$$

where the hat denotes an estimation, $\hat{\mathbf{e}}$ is a vector with a length equal to NEM and $\mathbf{F}$ is a vector equal to the number of DOFs (nDOF), and $\mathbf{B}_\mathrm{measured,b}$ and $\mathbf{K}$ are matrices of sizes NEM $\times$ nDOF and nDOF $\times$ nNDOF, respectively.

3.2 Damage detection and localization

Damage characterization in the plate can be obtained through the temporal comparison of updated values in $\mathbf{K}$, which values are represented through a reduction parameter ζ, as diagrammed in Figure 3. Matrix $\mathbf{K}$ is updated by minimizing the objective function J:

$$J = \|\hat{\mathbf{e}} - \mathbf{e}\|_2 \tag{15}$$

where $\| \cdot \|_2$ is L_2 norm and $\mathbf{e}$ is the mean of the observed strain field, which is obtained by averaging over a number of observations. In this present work, there is no additional inequality or equality constrains, except for the bound $[0, 1]$ on ζ. When $\zeta = 0$, the structural element has no damage, and conversely, when $\zeta = 1$ the structural element is removed (i.e. complete damage). Equation 15 is a nonlinear, multiple parameters function. For the purpose of this work, the pattern search solver in MATLAB[27] was used to solve the optimization problem through the minimization of the error, J. Convergence thresholds for either ζ or J were set to

$$\|\zeta^{i+1} - \zeta^i\| \le 10^{-8} \quad \text{or} \quad \|J^{i+1} - J^i\| \le 10^{-8} \tag{16}$$

and were used as the stop criteria for the optimization (Equation 15).

4. NUMERICAL EXAMPLE

This section numerically demonstrates the proposed algorithm.

4.1 Model Description

This numerical example considers a rectangular aluminum plate 1000 mm long by 500 mm wide and 3.3 mm thick. The model is clamped (i.e., fixed) on the right-hand side and a roller support is used on the left-hand side, and has a Young's modulus $E = 69$ GPa and a Poisson's ratio $\nu = 0.33$. For this preliminary work, the numerical representation of the plate was constructed using 50 elements, where 40 SECs are simulated with one SEC installed at the center of each element covering the majority of the element plus five boundary elements for each side without SECs). The Figure 4 is a schematic of the 50 elements showing the 40 SECs (darker squares) and 10 boundary elements (light rectangles).

Damage was introduced in the plate in the form of a reduction in stiffness at two different locations. The Young's modulus in the rectangular elements denoted as "damage a" and "damage b" in Figure 4 were reduced by 20% ($\zeta = 0.2$) and 40% ($\zeta = 0.4$), respectively. To investigate the effect of noise on the system, four levels of noise investigated: 1% uniformly distributed, 1% Gaussian, 3% Gaussian, and 5% Gaussian. A unit concentrated force was applied to a node near the center of the plate, as shown in Figure 4.
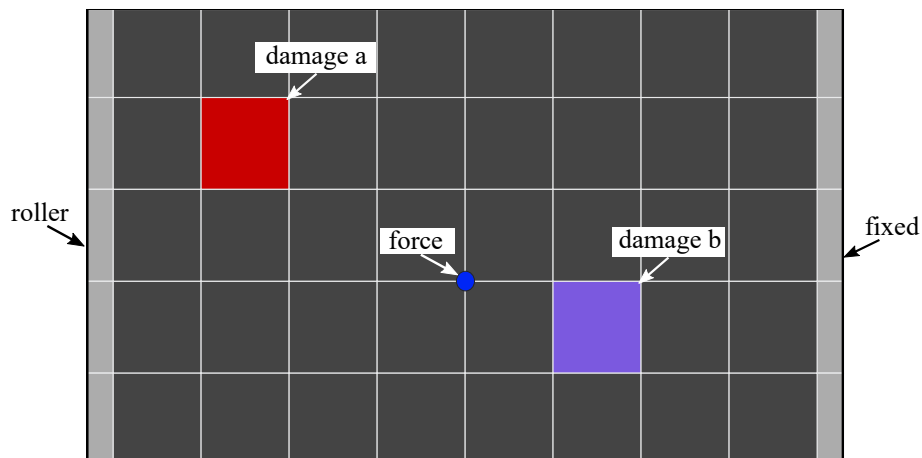
Figure 4. Schematic of the numerical example.

4.2 Numerical Results

Figure 5 shows the spatial distribution of ζ obtained through the algorithm. When inspecting results from the low-noise levels presented in Figures 5(a) and (b), it can be observed that the optimization technique was capable of correctly quantifying the reduction in stiffness for "damage a" as $\zeta = 0.4$ and "damage b" as $\zeta = 0.2$. Also, results show that while increasing the noise level reduces the precision of the damage localization, the algorithm can still identify and quantify both damage locations.
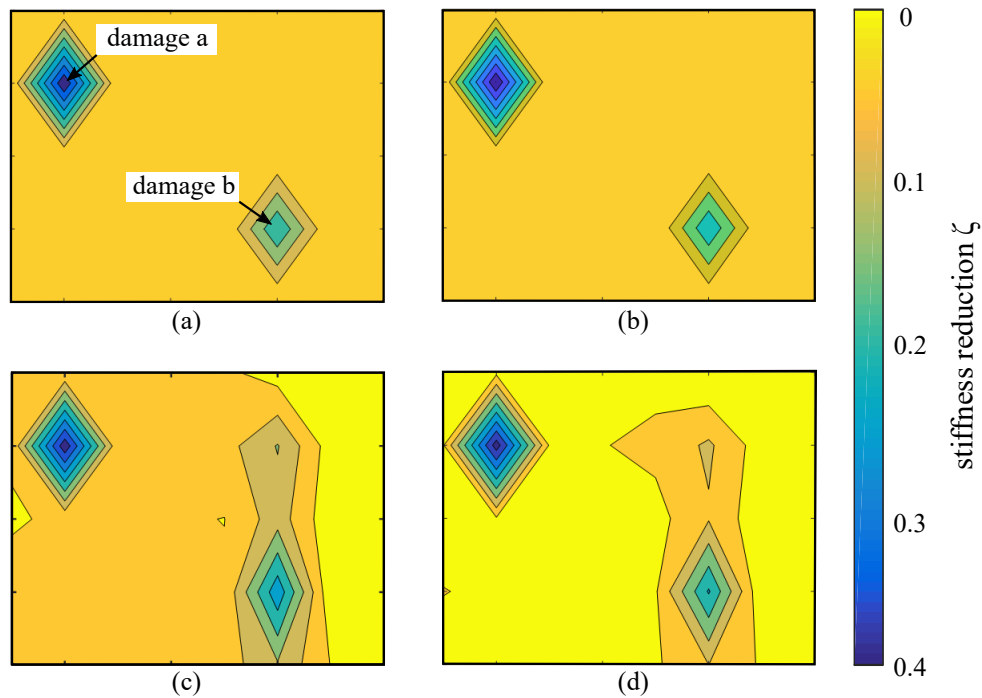
Figure 5. Contour plots of the identified stiffness reduction values for a noise level of: (a) 1% uniform; (b) 1% Gaussian; (c) 3% Gaussian; and (d) 5% Gaussian.

5. CONCLUSION

This work proposed and derived a physics-driven approach bespoke to components equipped with sensing skin providing additive strain measurements. The sensor forming the sensing skin, termed the soft elastomeric capacitor (SEC), is a large-scale strain sensor that is designed to cover large surfaces at low cost. The surrogate model presented in this work allows for the SEC's additive strain measurement to be mapped to structural stiffness. This is done by updating the stiffness matrix to match the strain measurements through a minimization function. A temporal comparison of the obtained stiffness matrix can be used for condition assessment, and the surrogate model itself could be useful to conduct further studies such as structural behavior prediction and remaining useful life estimation.

A numerical demonstration was conducted on a steel plate with a simulated dense sensor network of 40 SECs. Results showed that the proposed surrogate model could be used to detect, localize, and quantify damage, even in the presence of noise. Future work will involve validating the surrogate model technique through the use of higher fidelity finite element models and experimental data, and extend the methodology to dynamic excitations with uncertain loads.

ACKNOWLEDGMENTS

REFERENCES

[1] Koch, C., Georgieva, K., Kasireddy, V., Akinci, B., and Fieguth, P., "A review on computer vision based defect detection and condition assessment of concrete and asphalt civil infrastructure," *Advanced Engineering Informatics* **29**, 196–210 (apr 2015).

[2] Kim, J., Gucunski, N., Duong, T. H., and Dinh, K., "Three-dimensional visualization and presentation of bridge deck condition based on multiple NDE data," *Journal of Infrastructure Systems* **23**, B4016012 (sep 2017).

[3] Papaelias, M., Cheng, L., Kogia, M., Mohimi, A., Kappatos, V., Selcuk, C., Constantinou, L., Muoz, C. Q. G., Marquez, F. P. G., and Gan, T.-H., "Inspection and structural health monitoring techniques for concentrated solar power plants," *Renewable Energy* **85**, 1178 – 1191 (2016).

[4] Agdas, D., Rice, J. A., Martinez, J. R., and Lasa, I. R., "Comparison of visual inspection and structural-health monitoring as bridge condition assessment methods," *Journal of Performance of Constructed Facilities* **30**, 04015049 (jun 2016).

[5] Guo, T., Frangopol, D. M., and Chen, Y., "Fatigue reliability assessment of steel bridge details integrating weigh-in-motion data and probabilistic finite element analysis," *Computers & Structures* **112-113**, 245–257 (dec 2012).

[6] Liu, X., Dong, X., and Wang, Y., "Field testing of martlet wireless sensing system on an in-service prestressed concrete highway bridge," in [*Health Monitoring of Structural and Biological Systems 2016*], Kundu, T., ed., SPIE (apr 2016).

[7] Shafiullah, G. M., Ali, A. B. M. S., Thompson, A., and Wolfs, P. J., "Predicting vertical acceleration of railway wagons using regression algorithms," *IEEE Transactions on Intelligent Transportation Systems* **11**, 290–299 (jun 2010).

[8] Márquez, F. P. G., Tobias, A. M., Pérez, J. M. P., and Papaelias, M., "Condition monitoring of wind turbines: Techniques and methods," *Renewable Energy* **46**, 169–178 (2012).

[9] Farrar, C. R. and Sohn, H., "Pattern recognition for structural health monitoring," in [*Workshop on Mitigation of Earthquake Disaster by Advanced Technologies*], (2000).

[10] Gullapalli, H., Vemuru, V. S. M., Kumar, A., Botello-Mendez, A., Vajtai, R., Terrones, M., Nagarajaiah, S., and Ajayan, P. M., "Flexible piezoelectric ZnO-paper nanocomposite strain sensor," *Small* **6**, 1641–1646 (jul 2010).

[11] Glisic, B. and Inaudi, D., "Development of method for in-service crack detection based on distributed fiber optic sensors," *Structural Health Monitoring: An International Journal* **11**, 161–171 (aug 2011).

[12] Arsenault, T. J., Achuthan, A., Marzocca, P., Grappasonni, C., and Coppotelli, G., "Development of a FBG based distributed strain sensor system for wind turbine structural health monitoring," *Smart Materials and Structures* **22**, 075027 (jun 2013).

[13] Glii, B., Yao, Y., Tung, S. T. E., Wagner, S., Sturm, J. C., and Verma, N., "Strain sensing sheets for structural health monitoring based on large-area electronics and integrated circuits," *Proceedings of the IEEE* **104**, 1513–1528 (Aug 2016).

[14] Kang, I., Schulz, M. J., Kim, J. H., Shanov, V., and Shi, D., "A carbon nanotube strain sensor for structural health monitoring," *Smart Materials and Structures* **15**, 737–748 (apr 2006).

[15] Laflamme, S., Kollosche, M., Connor, J. J., and Kofod, G., "Robust flexible capacitive surface sensor for structural health monitoring applications," *Journal of Engineering Mechanics* **139**, 879–885 (jul 2013).

[16] Downey, A., Laflamme, S., and Ubertini, F., "Experimental wind tunnel study of a smart sensing skin for condition evaluation of a wind turbine blade," *Smart Materials and Structures* **26**, 125005 (oct 2017).

[17] Downey, A., Laflamme, S., and Ubertini, F., "Reconstruction of in-plane strain maps using hybrid dense sensor network composed of sensing skin," *Measurement Science and Technology* **27**, 124016 (nov 2016).

[18] Sanayei, M. and Saletnik, M. J., "Parameter estimation of structures from static strain measurements. i: Formulation," *Journal of Structural Engineering* **122**, 555–562 (may 1996).

[19] Sanayei, M. and Saletnik, M. J., "Parameter estimation of structures from static strain measurements. II: Error sensitivity analysis," *Journal of Structural Engineering* **122**, 563–572 (may 1996).

[20] Cerracchio, P., Gherlone, M., Sciuva, M. D., and Tessler, A., "A novel approach for displacement and stress monitoring of sandwich structures based on the inverse finite element method," *Composite Structures* **127**, 69–76 (sep 2015).

[21] Zhu, D., Dong, X., and Wang, Y., "Substructure stiffness and mass updating through minimization of modal dynamic residuals," *Journal of Engineering Mechanics* **142**, 04016013 (may 2016).

[22] Cancelli, A., Micheli, L., Laflamme, S., Alipour, A., Sritharan, S., and Ubertini, F., "Damage location and quantification of a pretensioned concrete beam using stochastic subspace identification," in [*Nondestructive Characterization and Monitoring of Advanced Materials, Aerospace, and Civil Infrastructure 2017*], Wu, H. F., Gyekenyesi, A. L., Shull, P. J., and Yu, T.-Y., eds., SPIE (apr 2017).

[23] Saleem, H., Thunga, M., Kollosche, M., Kessler, M., and Laflamme, S., "Interfacial treatment effects on behavior of soft nano-composites for highly stretchable dielectrics," *Polymer* **55**(17), 4531–4537 (2014).

[24] Laflamme, S., Ubertini, F., Saleem, H., D'Alessandro, A., Downey, A., Ceylan, H., and Materazzi, A. L., "Dynamic characterization of a soft elastomeric capacitor for structural health monitoring," *Journal of Structural Engineering* **141**, 04014186 (aug 2015).

[25] Reddy, J., [*An Introduction to the Finite Element Method*], McGraw-Hill, 3 ed. (2005).

[26] Kefal, A., Oterkus, E., Tessler, A., and Spangler, J. L., "A quadrilateral inverse-shell element with drilling degrees of freedom for shape sensing and structural health monitoring," *Engineering Science and Technology, an International Journal* **19**(3), 1299 – 1313 (2016).

[27] "Matlab optimization toolbox," (2017a). The MathWorks, Natick, MA, USA.